Substrate Integrated Monopulse Leaky Horn Antenna

Cleofás Segura-Gómez, Lei Wang, *Senior Member, IEEE,* Andrés Biedma-Pérez, Ángel Palomares-Caballero, Pablo Padilla

***Abstract*—This paper presents a leaky horn antenna based on a substrate integrated waveguide (SIW) with monopulse performance. The proposed leaky horn antenna consists of two SIW leaky-wave antennas (LWAs) angularly separated to form the horn's flaring. By properly designing this angular separation taking into account the main radiation direction of both LWAs, a flat wavefront is achieved in the leaky horn aperture. To provide the monopulse behavior to the SIW leaky horn, a hybrid coupler, and phase shifters are included in the feeding. Depending on the input port chosen on the hybrid coupler, the LWAs forming the leaky horn are fed in phase or counter-phase and generate the sum and difference radiation patterns. A prototype has been fabricated to validate the design. In the operating band, an impedance matching below −13.9 dB is achieved at both input ports with an isolation between ports better than 16.6 dB. The measured radiation patterns show a monopulse behavior with a proper agreement with the simulated results. The proposed leaky horn presents a depth of −25.8 dB (difference between the sum diagram and the difference in the boresight axis), a peak realized gain of 12.9 dBi, and a half-power beamwidth of 6.4° at 27.5 GHz.**

***Index Terms*—Horn antenna, hybrid coupler, leaky-wave antenna (LWA), monopulse antenna, substrate integrated waveguide (SIW).**

I. Introduction

MONOPULSE antennas are a fundamental part of some radar systems. This type of antenna enables accurate tracking through a single pulse towards the antenna boresight (AB) [1]. For this purpose, the antenna system consists of multiple antennas which are symmetrical concerning the AB. Typically, a group of four antennas is used for the estimation in the two main planes. However, a only group of two antennas is enough to estimate on a single plane [2], [3]. When the two antennas of the group are fed by the same signal, a sum pattern (Σ) is achieved with a maximum in the AB. On the other hand, when they are fed in counter-phase, the difference pattern (Δ) has a null in the AB. The combination of both patterns gives the target angular position around AB.

This work has been supported by grant TED2021-129938B-I00 funded by MCIN/AEI/10.13039/501100011033 and by the European Union NextGenerationEU/PRTR. It has also been supported by grants PDC2023-145862-I00, PDC2022-133900-I00, PID2020-112545RB-C54, and TED2021-131699B-I00, and by "Ministerio de Universidades" through grant FPU20/00256 and EST23/00141.

Cleofás Segura-Gómez, Andrés Biedma-Pérez, Ángel Palomares-Caballero, and Pablo Padilla are with the Department of Signal, Telematics, and Communications. Research Centre for Information and Communication Technologies (CITIC). University of Granada, Granada, Spain (emails: cleofas@ugr.es, abieper@ugr.es, angelpc@ugr.es, pablopadilla@ugr.es).

Lei Wang is with the School of Engineering, Lancaster University, Lancaster, United Kingdom (e-mail: wanglei@ieee.org).

The implementation of monopulse antennas can be done in different technologies such as microstrip [2], waveguide [4], or gap-waveguide [5]. Nevertheless, a preferred option for monopulse antennas is the substrate integrated waveguide (SIW) due to its low cost, low profile, and reduction of radiation losses when the frequency increases. In the literature, there are several works of SIW monopulse antennas designed as 1-D [6]–[8] or 2-D arrays [9]–[13]. All of the above works have the feature in common of providing a broadside radiation pattern. This may be a drawback for some military and commercial applications where antennas with end-fire radiation are needed [14]. For example, to facilitate mounting on a platform while maintaining a low profile, or to provide radiation parallel to the surface [15]. End-fire monopulse antennas in SIW have been less explored and only a few examples have been reported. In [16], the monopulse performance is achieved by using two antipodal linearly tapered slot antennas (ALTSA) and a directional coupler in SIW. The design process of the previous work may become complex if more antennas are needed to increase the receiving physical aperture. Another SIW end-fire monopulse antenna design is presented in [17], in which an array of four printed Yagi antennas are fed by an SIW hybrid ring coupler and power dividers. Increasing the number of antenna elements in the array would require increasing the number of power dividers, which implies a careful design to keep low the reflection coefficient [18]. In [19], an alternative design for generating SIW end-fire monopulse antennas is presented through the combined use of a phase-corrected SIW horn and ALTSAs. However, the generation of the Σ and Δ patterns is produced by different SIW antennas, which incurs in a bulkier system, for which the aperture for reception is physically separated. In addition, the radiation patterns of the previously SIW monopulse antennas are horizontally polarized, being parallel to the surface. This is not the preferred

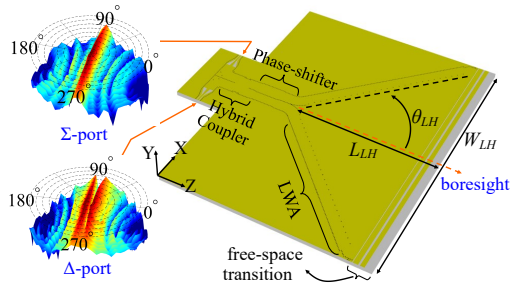

Fig. 1. Visual summary: design of the proposed SIW end-fire monopulse LH, and its measured 3D farfield radiation patterns at 28 GHz. Dimensions: W_{LH} = 98.9 mm, L_{LH} = 50.5 mm, θ_{LH} = 45°.

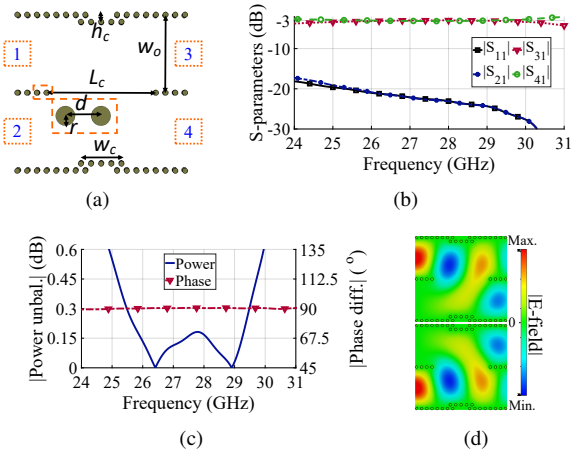

Fig. 2. SIW hybrid coupler: (a) design, (b) S-parameters: reflection (port 1), isolation (port 2) and transmission (port 3 and 4) from port 1, (c) power imbalance and phase difference between output ports (in absolute value), and (d) E-field at 28 GHz when fed by the input ports. Dimensions are: r = 0.15 mm, d = 0.55 mm, w_o = 4.4 mm, L_c = 6.2 mm, h_c = 0.3 mm, w_c = 2.3 mm.

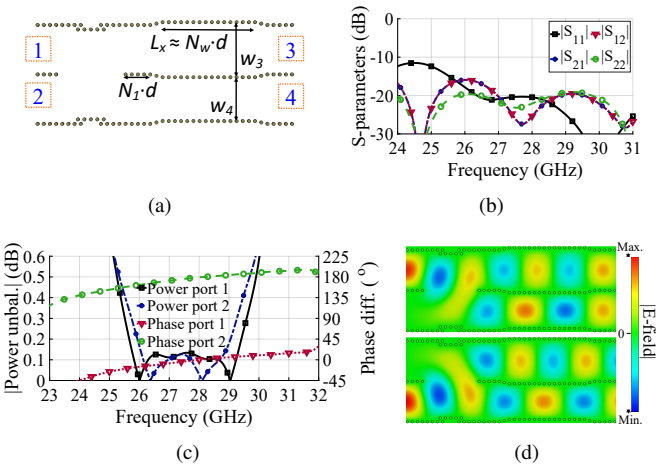

Fig. 3. Hybrid coupler plus phase shifters: (a) design, and (b) S-parameters. S_{3X} - S_{4X} calculated for each input port: (c) Absolute power difference, and phase difference. (d) E-field at 28 GHz when fed by the input ports. Dimensions are: w_3 = 4.9 mm, w_4 = 3.9 mm, N_1 = 5, N_w = 16.

polarization for radar applications, where vertical polarization is more suitable due to a stable propagation characteristic and reduced loss by the ground reflection [20].

Recently, a new design concept has been introduced named leaky horn (LH) [21], [22]. It combines the main features of leaky-wave antennas (LWAs) and horn antennas in the same device. LWAs provide a customizable radiation pattern while their integration into a horn antenna simplifies the feeding to provide high directivity. In addition, having the two LWAs can provide great potential as they can be designed in a complementary way to obtain the desired radiation pattern. So far, only a couple of LH designs have been presented [22], although none of them have exploited their potential to conceive monopulse antennas. This letter presents for the first time an SIW end-fire monopulse antenna based on LH.

II. Monopulse LH Antenna

This section details the design of the proposed SIW monopulse antenna shown in Fig. 1. The considered laminate is RO4003C with a design relative permittivity ε_r of 3.55 and a loss tangent tanδ of 0.0027 at 10 GHz. The substrate thickness is 1.524 mm with a 35 μm copper cladding on each side. The simulations have been performed using CST Studio.

A. Hybrid Coupler and Phase Shifter

The monopulse LH antenna illustrated in Fig. 1 incorporates two input ports labeled as Σ- and Δ-ports. Depending on the input port selected, the LH produces the Σ- or Δ-patterns. To achieve the described behavior, it is necessary to employ an SIW hybrid coupler and a phase shifter after the input ports. The designed SIW hybrid coupler is shown in Fig. 2(a). There are several configurations to obtain a hybrid coupler, but this design follows the work in [23], which is the SIW version of Riblet's coupler [24]. It is a four-port component that allows a compact -3 dB power division from the two input ports (ports 1 and 2) towards the two output ports (ports 3 and 4). In addition, each input port must be isolated from the other to avoid interference in the power received by the Σ- and Δ-ports. Due to the symmetry of the SIW hybrid coupler, the S-parameters are symmetrical and it is only analyzed the performance when port 1 is fed. Fig. 2(b) shows the reflection parameter ($|S_{11}|$) and the isolation parameter ($|S_{21}|$). From 25.5 GHz to 29.5 GHz, $|S_{11}|$ and $|S_{21}|$ are below -18 dB, while the transmission parameters ($|S_{31}|$ and $|S_{41}|$) is around -3 dB. In Fig. 2(c), it is presented the absolute power imbalance and the phase difference between the output ports from any input port. In the previously referred frequency range, the power imbalance is lower than 0.3 dB and the absolute phase difference is 90° ensuring the proper operation. Nevertheless, it is important to note that the resulting phase difference between output ports (taking port 4 as a reference) is: $-90°$ (delay) feeding from the input port 1, and $+90°$ (advance) for the input port 2. This effect can be verified by the electric field (E-field) shown in Fig. 2(d). However, to ensure monopulse behavior, it is necessary to obtain a phase difference between the output ports of 0° and 180°, respectively. Therefore, an additional SIW section needs to be placed after the output ports in order to reduce the phase shift when fed by port 1 and increase it when fed by port 2.

A simple but effective method to generate phase shifts in SIW is by modifying the width of the waveguide section. Fig. 3(a) shows the previous SIW hybrid coupler with the SIW phase shifters after each output port. Different widths w_3 and w_4 with the same length L_x for the phase shifters are considered. Based on this design, it is possible to adjust w_3, w_4 and L_x to obtain the desired phase shift between the output ports ($+90°$). The phase shift provided by each SIW phase shifter regarding the reference SIW is computed as follows:

$$\varphi_i = L_x \cdot \left(\sqrt{k^2 - \left(\frac{\pi}{w_o}\right)^2} - \sqrt{k^2 - \left(\frac{\pi}{w_i}\right)^2} \right); \quad i = 3, 4 \quad (1)$$

where $k = 2\pi\sqrt{\varepsilon_r}/\lambda_o$, and w_i indicates the width of each SIW phase shifter. The required phase shifts are $\varphi_3 = -45°$ and $\varphi_4 = +45°$. The resulting design to achieve the target

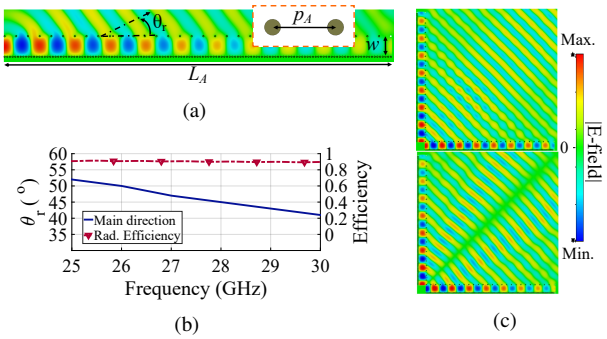

Fig. 4. (a) E-field in the single SIW LWA, (b) main radiating direction of the single LWA, and its radiation efficiency, and (c) E-field at 28 GHz in an LH with a phase shift of 0º and 180º between both LWAs. Dimensions are: W = 3.8 mm, L_A = 60 mm, p_A = 2.2 mm.

φ_3 and φ_4 values is shown in Fig. 3(a). The design has some asymmetry, resulting in different reflection parameters for the input ports but with the same isolation. The S-parameters of the hybrid coupler and phase shifters are presented in Fig. 3. The transmission parameters are omitted as they are similar to the ones displayed in Fig. 2(b). Nevertheless, Fig. 3(c) shows the power imbalance and the phase difference between output ports. Due to the frequency dependence of the phase shifters, there is a maximum phase imbalance in the operation range of less than 20.0º at 25.7 GHz. The power imbalance is below 0.3 dB from 25.7 GHz to 29.3 GHz. Regarding the phase difference, it is obtained a 0º phase shift for the input port 1 and a 180º phase shift for the input port 2. Fig. 3(d) shows the response illustrating the propagating E-field.

B. LH Antenna Design

Following the design depicted in Fig. 1, the outputs of the SIW phase shifters are connected to the inputs of two SIW LWAs forming the LH. For simplicity in demonstrating the LH concept, the LWAs chosen are a uniform LWA whose design together with the leaky field is shown in 4(a). This implies that one of the lateral walls of the SIW produces leakage by a uniform spacing p_A of the metalized vias. The main angular direction of radiation of the SIW LWA [25] is computed as:

$$\theta_r \simeq \sin^{-1}\left(\frac{\beta}{k}\right) = \sin^{-1}\left(\sqrt{1-\left(\frac{\lambda_o}{2\,w_{ef}\sqrt{\varepsilon_r}}\right)^2}\right) \qquad (2)$$

where β is the phase constant of the fundamental mode in the SIW, while k is the wavenumber of the dielectric region that forms the horn's flaring. On the right-hand side of Eq. (2), it is possible to check the dependence of the variable w_{ef}, which refers to the effective width of the SIW that is going to be slightly larger than the physical width w [see Fig. 4(a)]. The larger p_A, the larger the w_{ef} one and hence, the value of θ_r [26]. The distance between the vias p_A also determines the attenuation constant α, which provides the amount of leakage per length unit. The value chosen for p_A has been set so as not to disturb too much the β value as well as to produce some leakage through uniformly spaced vias. Taking this into account, the length L_A of the LWA has been adjusted

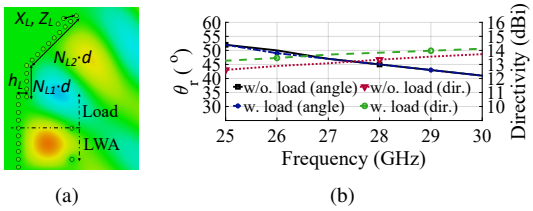

Fig. 5. SIW structure at the LWA end: (a) design and E-field at 28 GHz, and (b) main radiating direction and directivity over the frequency. Dimensions are: X_L = 0.2 mm, Z_L = 0.5 mm, h_L = 0.6 mm, N_{L1} = 5, N_{L2} = 6.

to radiate around 90% of the input power [25]. Due to the decay of the power in the waveguide by progressive radiation and losses, the radiation efficiency of the last gaps between the vias is not significant in the uniform LWA. Fig. 4(b) shows the radiation efficiency and radiation angle θ_r of the SIW LWA. At 28 GHz, θ_r is 45º with a radiation efficiency of 90%. In the considered band, variations of ± 5º for θ_r are observed due to the dispersive behavior of the LWAs.

Once the θ_r has been calculated, the LH's flaring angle θ_{LH} [see Fig. 1] is determined as $\theta_{LH} = 2\,\theta_r$ in order to provide the maximum directivity at the AB. In this design case, θ_{LH} is 90º. Fig. 4(c) shows the E-field in a 90º LH when both SIW LWAs are fed in-phase or counter-phase. The principle of operation of the LH is different from a traditional horn antenna, as the feeding is from the horn sides rather than from the focal point. Thanks to this, a nearly constant phase and amplitude are achieved in all sections of the horn, as can be observed for the in-phase feeding in Fig. 4(c). The simulations in Fig. 4(c) also demonstrate the monopulse behaviour of the proposed LH depending on the phase shift between the LWAs.

C. Transitions

To complete the design of LH and to develop a prototype, some transitions are needed either for proper feeding and for allowing efficient radiation, as indicated in Fig. 1. On the one hand, for the feeding, grounded coplanar-waveguide transitions [18] have been used in the Σ- and Δ-ports. On the other hand, for the radiation of the LH, an SIW-to-free space transition [18] has been included along the aperture. This transition is composed of pairs of dielectric slabs with and without metalization. The ratio of the non-metalized slot to the metalized strip increases for each pair, and in this case, the use of three pairs together with the control of the length of each pair is sufficient to match impedances over the target bandwidth. Additionally, at the end of the LWAs, a specific SIW structure has been placed to control the power that is not radiated along the LWAs. The design, which is depicted in Fig. 5(a), consists of an SIW bend that allows redirecting the remaining power to contribute in the wavefront direction. Moreover, two additional vias are included on the external side to avoid back radiation. Fig. 5(b) displays how this structure does not disturb θ_r and it increases the directivity.

III. Experimental Validation and Discussion

The manufactured prototype of the proposed SIW monopulse LH antenna is shown in Fig. 6(a). A comparison

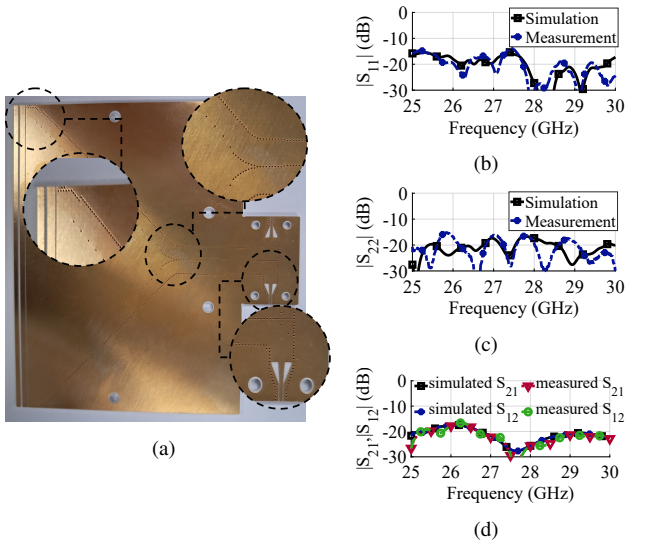

Fig. 6. (a) Manufactured SIW monopulse LH antenna. Reflection coefficients of the: (b) the Σ-port and, (c) the Δ-port. (d) Isolation between Σ and Δ-port.

between simulated and measured S-parameters is presented in Figs. 6(b) - 6(d). A proper agreement can be observed for the reflection coefficients of the Σ and Δ ports with a value below -13.9 dB in the considered band. The isolation between both input ports is also acceptable, being below -16.6 dB.

The radiation performance of the proposed LH design can be seen in Fig. 7, which shows a comparison between simulated and measured H-plane Σ and Δ radiation patterns at several frequencies. It is possible to confirm a high correspondence between simulations and measurements, demonstrating the monopulse behavior of the proposed LH. Regarding the null depth (ND), which is the difference between the Σ and Δ radiation patterns at AB, it is lower than -25.8 dB for the center frequency. This ND value is lower even at other frequencies in the considered bandwidth. Another important characteristic for discrimination in radar applications is the beamwidth that achieves a value of 6.4° at the central frequency. Fig. 7(c) shows the measured cross-polarization normalized to the maximum of the co-polar level of its corresponding radiation pattern. The cross-polarization level is below -25 dB around the maxima of the co-polar radiation patterns. Fig. 8(a) displays the simulated directivity alongside the simulated and measured realized gain at AB. Both gains are similar in the working frequency band and are around 2.7 dB below directivity, mainly due to dielectric losses of the substrate at these frequencies, as shown by the efficiencies in Fig. 8(b). There is only a small deviation of the working frequency band between the simulation and the measurement due to manufacturing tolerances, mostly affected by the actual relative permittivity. In the considered range, the gain is greater than 10.7 dBi, and outside, the LH suffers from the inherent dispersion of the LWAs reducing the directivity.

Finally, Table I presents the comparison with the existing SIW monopulse end-fire antennas in the literature. The proposed LH design achieves a similar and even higher realized gain than the compared works for the Σ and Δ radiation patterns. However, the presented LH design provides a smaller

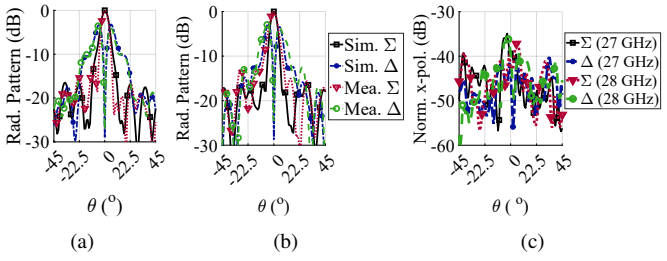

Fig. 7. Normalized simulated and measured Σ and Δ co-polarization radiation patterns at H-plane (XZ plane in Fig. 1.) for: (a) 27 GHz, and (b) 28 GHz. (c) Measured Σ and Δ cross-polarization radiation patterns at H-plane.

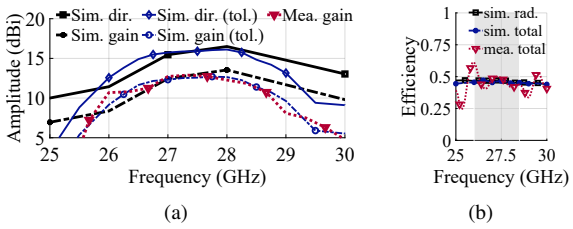

Fig. 8. (a) Simulated directivity, simulated realized gain both without and with adjusted tolerances, and measured realized gain for Σ-port. (b) Simulated radiation and total efficiencies, and measured total efficiency.

TABLE I
COMPARISON WITH OTHER SIW MONOPULSE END-FIRE ANTENNAS

Ref.	Freq. (GHz) / Bandwidth	Max. gain $\Sigma - \Delta$ (dBi)	Beamwidth 3-dB	ND (dB)	Pol.	Aperture length
[16]	36 / (13.69%)	10.6 – 7.6	22.5°	−35	H-pol	$1.8\lambda_\circ$
[17]	10 / (7.2%)	13.1 – 10.4	12°	−33.8	H-pol	$3.35\lambda_\circ$
[19]	10.1 / (5.8%)	12.84 – 8.77	18.6°	−44.24	H-pol	$2.69\lambda_\circ$
This	27.4 / (10.2%)	12.9 – 10.0	6.4°	−25.8	V-pol	$7.91\lambda_\circ$

3-dB beamwidth due to the use of an aperture with a longer electrical length. For the referred works, increasing the physical aperture leads to the inclusion of a larger number of power dividers to realize a feeding corporate network. In our proposed design, the achievable physical aperture depends on the SIW LWA radiation angle θ_r as is described in section II.B. At the central operation frequency, the larger θ_r, the larger the physical aperture and hence the directivity provided. In addition, the proposed LH monopulse is the only one so far that allows for radiating with vertical polarization.

IV. Conclusion

An end-fire monopulse LH antenna based on SIW technology has been presented. Due to the flexibility in the independent feeding of both LWAs forming the LH, Σ and Δ radiation patterns with high directivity can be generated. The in-phase and counter-phase feedings of both LWAs, depending on the input port, have been achieved compactly by the combined use of a hybrid coupler and phase shifters. The fabricated SIW leaky horn experimentally demonstrates the monopulse behavior for an electrically large aperture without the use of a large number of power dividers. This feature is the main advantage over existing SIW end-fire monopulse antenna designs in addition to the produced vertical polarization which is advantageous in radar applications.

REFERENCES

[1] S. M. Sherman and D. K. Barton, *Monopulse principles and techniques*. Artech House, 2011.

[2] Z.-W. Yu, G.-M. Wang, and C.-X. Zhang, "A broadband planar monopulse antenna array of *c*-band," *IEEE Antennas Wireless Propag. Lett.*, vol. 8, pp. 1325–1328, 2009.

[3] L. Polo-López, J. Córcoles, J. A. Ruiz-Cruz, J. R. Montejo-Garai, and J. M. Rebollar, "Triple-radiation pattern monopulse horn feed with compact single-layer comparator network," *IEEE Trans. Antennas Propag.*, vol. 69, no. 5, pp. 2546–2559, 2021.

[4] E. Garcia-Marin, J.-L. Masa-Campos, and P. Sanchez-Olivares, "Diffusion-bonded W-band monopulse array antenna for space debris radar," *AEU-Int. J. Electron. Commun.*, vol. 116, p. 153061, 2020.

[5] M. Ferrando-Rocher, J. I. Herranz-Herruzo, A. Valero-Nogueira, and B. Bernardo-Clemente, "All-metal monopulse antenna array in the Ka-band with a comparator network combining ridge and groove gap waveguides," *IEEE Antennas Wireless Propag. Lett.*, vol. 22, no. 6, pp. 1381–1385, 2023.

[6] H. Chu, J.-X. Chen, S. Luo, and Y.-X. Guo, "A millimeter-wave filtering monopulse antenna array based on substrate integrated waveguide technology," *IEEE Trans. Antennas Propag.*, vol. 64, no. 1, pp. 316–321, 2015.

[7] J. Soleiman Meiguni, S. A. Khatami, and A. Amn-e Elahi, "Compact substrate integrated waveguide mono-pulse antenna array," *Int. J. RF Microw. Comput. Aided Eng.*, vol. 28, no. 1, p. e21155, 2018.

[8] J.-Y. Deng, L.-Q. Luo, and J.-Y. Yin, "Bidirectionally-fed slow-wave substrate-integrated waveguide monopulse slot array antenna with gain enhancement," *IEEE Antennas Wireless Propag. Lett.*, vol. 22, no. 12, pp. 2856–2860, 2023.

[9] B. Liu, W. Hong, Z. Kuai, X. Yin, G. Luo, J. Chen, H. Tang, and K. Wu, "Substrate integrated waveguide (SIW) monopulse slot antenna array," *IEEE Trans. Antennas Propag.*, vol. 57, no. 1, pp. 275–279, 2009.

[10] F. Cao, D. Yang, J. Pan, D. Geng, and H. Xiao, "A compact single-layer substrate-integrated waveguide (SIW) monopulse slot antenna array," *IEEE Antennas Wireless Propag. Lett.*, vol. 16, pp. 2755–2758, 2017.

[11] J. Zhu, S. Liao, S. Li, and Q. Xue, "60 GHz substrate-integrated waveguide-based monopulse slot antenna arrays," *IEEE Trans. Antennas Propag.*, vol. 66, no. 9, pp. 4860–4865, 2018.

[12] T. Yang, Z. Zhao, D. Yang, X. Liu, and Q.-H. Liu, "A single-layer SIW slots array monopulse antenna excited by a dual-mode resonator," *IEEE Access*, vol. 7, pp. 131 282–131 288, 2019.

[13] Z. Sun, S. Liu, Y. Yang, X. Zheng, J. Wang, W. He, T. An, and X. Zhao, "A dual-polarized 2-D monopulse antenna array based on substrate integrated waveguide," *IEEE Trans. Antennas Propag.*, vol. 70, no. 12, pp. 11 771–11 778, 2022.

[14] Y. Cao, Y. Cai, L. Wang, Z. Qian, and L. Zhu, "A review of substrate integrated waveguide end-fire antennas," *IEEE Access*, vol. 6, pp. 66 243–66 253, 2018.

[15] Y. Hou, Y. Li, Z. Zhang, and M. F. Iskander, "All-metal endfire antenna with high gain and stable radiation pattern for the platform-embedded application," *IEEE Trans. Antennas Propag.*, vol. 67, no. 2, pp. 730–737, 2019.

[16] Y. J. Cheng, W. Hong, and K. Wu, "Design of a monopulse antenna using a dual V-type linearly tapered slot antenna (DVLTSA)," *IEEE Trans. Antennas Propag.*, vol. 56, no. 9, pp. 2903–2909, 2008.

[17] X. Zou, C.-M. Tong, J.-S. Bao, and W.-J. Pang, "SIW-fed Yagi antenna and its application on monopulse antenna," *IEEE Antennas Wireless Propag. Lett.*, vol. 13, pp. 1035–1038, 2014.

[18] C. Segura-Gómez, Á. Palomares-Caballero, and P. Padilla, "A 1-to-8 fully modular stacked SIW antenna array for millimeter-wave applications," *IEEE Trans. Antennas Propag.*, vol. 70, no. 11, pp. 11 149–11 154, 2022.

[19] L. Wang, X. Yin, and H. Zhao, "A planar feeding technology using phase-and-amplitude-corrected SIW horn and its application," *IEEE Antennas Wireless Propag. Lett.*, vol. 14, pp. 147–150, 2015.

[20] W. Diao, R. Li, Y. Li, and Z. Zhang, "An ultrawideband H-plane monopulse log-periodic antenna for jamming signal finding," *IEEE Trans. Antennas Propag.*, vol. 72, no. 9, pp. 7305–7310, 2024.

[21] L. Wang and G. Goussetis, "Leaky wave fed substrate integrated horn antenna," in *2020 13th UK-Europe-China Workshop on Millimetre-Waves and Terahertz Technologies (UCMMT)*. IEEE, 2020, pp. 1–3.

[22] D. Zheng, K. Wu, and W. Hong, "Leaky horns: A new paradigm of developing electromagnetic horns based on leaky-wave structures," *Electromagnetic Science*, vol. 2, pp. 1–4, 2024.

[23] B. Liu, W. Hong, Z. C. Hao, and K. Wu, "Substrate integrated waveguide 180-degree narrow-wall directional coupler," in *2005 Asia-Pacific Microwave Conference Proceedings*, vol. 1. IEEE, 2005, pp. 3–pp.

[24] H. J. Riblet, "The short-slot hybrid junction," *Proc. IRE*, vol. 40, no. 2, pp. 180–184, 1952.

[25] D. R. Jackson and A. A. Oliner, *Leaky-Wave Antennas*. John Wiley & Sons, Ltd, 2008, ch. 7, pp. 325–367.

[26] A. J. Martinez-Ros, J. L. Gomez-Tornero, and G. Goussetis, "Planar leaky-wave antenna with flexible control of the complex propagation constant," *IEEE Trans. Antennas Propag.*, vol. 60, no. 3, pp. 1625–1630, 2012.